

On the corrections to Strong-Stretching Theory for end-confined, charged polymers in a uniform electric field

Gabriele Migliorini¹

*Department of Mathematics, University of Reading,
Whiteknights, Reading RG6 6AX, United Kingdom*

We investigate the properties of a system of semi-diluted polymers in the presence of charged groups and counter-ions, by means of self-consistent field theory. We study a system of polyelectrolyte chains grafted to a similarly, as well as an oppositely charged surface, solving a set of saddle-point equations that couple the modified diffusion equation for the polymer partition function to the Poisson-Boltzmann equation describing the charge distribution in the system. A numerical study of this set of equations is presented and comparison is made with previous studies. We then consider the case of semi-diluted, grafted polymer chains in the presence of charge-end-groups. We study the problem with self-consistent field as well as strong-stretching theory. We derive the corrections to the Milner-Witten-Cates (MWC) theory for weakly charged chains and show that the monomer-density deviates from the parabolic profile expected in the uncharged case. The corresponding corrections are shown to be dictated by an Abel-Volterra integral equation of the second kind. The validity of our theoretical findings is confirmed comparing the predictions with the results obtained within numerical self-consistent field theory.

PACS numbers: 61.25.H Macromolecular and polymer solutions; 41.10.D Electrostatics, magnetostatics

I. INTRODUCTION

The stability of a dispersion against coagulation has been one of the primary subjects of research in colloid science. Colloidal stability can be obtained in polar solvents by means of ionic molecules. In this case an electrical double layer forms at the interface between the colloidal particles and the solvent, and the dependence of its structure on the electrolyte properties has been the key ingredient to explain electrostatic-induced colloidal stability in the past¹. In practice however electrostatic stability is difficult to obtain, due to extreme sensitivity of the process to the electrolyte conditions. A viable alternative to electrostatic stabilization is to adsorb or end-graft non-ionic polymers on the surface of colloidal particles^{2,3}. The stabilization mechanism obtained in this case is steric in nature. The theory of stabilization of colloids by adsorbed neutral polymers^{4,5} is one of the first problems where self-consistent field theory has been applied^{6,7}. Self-consistent field theory, introduced in the context of neutral polymer systems by Edwards⁸ and Helfand⁹, together with its discrete, lattice formulation counterpart¹⁰, has been applied and extended to a variety of inhomogeneous systems, including block-copolymer systems¹¹, polymers at interfaces, as well as non-ionic polymer brushes¹²⁻¹⁴. The study of polymer chains terminally attached to an interface has been branching from the colloidal science area to many other domains of research. Polymer brushes are a topic of interest in surface science, in view of their ability to modify surface properties¹⁵⁻¹⁷. In particular chain-end-functionalized polymer brushes, with uncharged¹⁸, as well as charged¹⁹⁻²¹ end-groups, have been used to design and control surface properties in a variety of dif-

ferent ways. Theoretical studies of charged-end-group brushes²², and their response to an electrical external field²³, have been discussed recently.

Polyelectrolytes are macromolecules containing ionizable groups. Their tendency to dissociate in solution into charged groups and low-molecular-weight counter-ions makes polyelectrolytes an interesting problem, as both steric interactions of the high-molecular-weight structure and electrostatic interactions between counter-ions and charged groups, coexist at different length scales. Due to the intricate interplay of these different type of interactions, the properties of polyelectrolyte solutions, as well as the behavior of polyelectrolytes near an interface, have been considerably more difficult to explain than those of non-ionic polymers. Extensions of the lattice self-consistent field theory for neutral polymers¹⁰ have been discussed²⁴. The self-consistent theory of inhomogeneous polyelectrolyte systems has been formulated^{25,26}, and recently reconsidered in the context of symmetric di-block polyelectrolytes and polyelectrolyte blends^{27,28}. As discussed in the past²⁹⁻³¹, for a system of end-grafted polyelectrolytes, the charge distribution is localized at the interface and symmetry considerations, as well as considerations about the double layer that forms at the surface, simplify their study. We consider both the case of end-grafted polyelectrolyte chains and end-grafted polymer chains with charged-end-groups at a flat interface, by means of self-consistent field theory. Related studies have been presented in the past^{22,32-34} and a detailed comparison of the results obtained within self-consistent field theory with the predictions of analytic strong-stretching theory³⁵ are discussed in this work. The conformational properties of the system in the presence of a uniform external field²³ are then addressed. The response of a polyelectrolyte brush to an external electric field repre-

sents an important problem with several practical applications. Its role in the actuation of nano-size cantilevers, to cite one of the many possible applications, has been recently reported³⁶. We study a system of end-confined charged polymer chains and its response to a uniform external field. We discuss the conformational changes of the monomer-density and counter-ion distribution profiles, for both the case of a similarly and oppositely charged grafting surface. We propose a new mathematical framework, that generalizes strong-stretching theory for charged grafted polymers in the presence of a uniform field and we discuss the results of our findings.

II. THEORY

We introduce in this section the theoretical methods to describe the properties of a polyelectrolyte system of chains attached to a flat interface. The system is composed of n_p polymers chains of length N_p , grafted to a flat, charged substrate of area \mathcal{A} with grafting density $\sigma = n_p/\mathcal{A}$, in the presence of a second surface, at a distance d and in the presence of n_c counter-ions of valence z_c in solution. We consider the case of strongly dissociating polyelectrolytes, so that the number and position of the charges along the polymer chains is fixed and determined by the ionization degree parameter f , the total charge per chain being fN_p . The charge distribution along the polymer will be referred as $z_p(s)$, s being the parameter that measures distance along the polymer backbone. Both the uniformly charged as well as the neutral brush with charged-end-groups are described by the present formalism. The ionization degree, polymer length and grafting density determine the counter-ion concentration, according to the electro-neutrality condition, $n_c z_c + fN_p n_p z_p = 0$. The presence of monovalent salt may easily be included in the notation introduced below, as well as the presence of other 'small' and polymeric charged species, according to the general formulation²⁵ discussed in Appendix A. Each polymer occupies a volume N_p/ρ_0 and has a natural end-to-end length of $aN_p^{1/2}$, a being the Kuhn segment. We assume all charged species, namely counter- and co-ions, to be point-like particles, neglecting steric contributions due to non-polymeric species. A general formulation of the theory, where several species are present and the size of the counter-ions and co-ions is explicitly taken into account, is discussed in Appendix A. The system is immersed in a solvent. As in the case of non-ionic systems, the corresponding degrees of freedom can be integrated out, so that the effective interaction between the monomers is described by the effective, short-ranged excluded-volume interaction parameter v . The Bjerrum length $l_B = e^2/\epsilon(\mathbf{r})k_B T$, together with the reference density ρ_0 and the excluded-volume parameter v , characterizes the properties of the system.

We consider in this section a single polyelectrolyte species in the presence of counter-ions, so that $N_p = N$

and $n_p = n$. The dimensionless counter-ion concentration is defined as

$$\hat{\phi}_c(\mathbf{r}) = \frac{1}{\rho_0} \sum_{\alpha=1}^{n_c} \delta(\mathbf{r} - \mathbf{r}_c^\alpha), \quad (1)$$

and the monomer concentration is defined as

$$\hat{\phi}_p(\mathbf{r}) = \frac{N}{\rho_0} \sum_{\alpha=1}^n \int_0^1 \delta(\mathbf{r} - \mathbf{r}_p^\alpha(s)) ds, \quad (2)$$

where the configuration of the α -th chain, belonging to the polymer species p is defined by the vector \mathbf{r}_p^α and where the position of the α -th counter-ion is given by \mathbf{r}_c^α .

The partition function associated with a system of polyelectrolyte chains in the presence of counter-ions, tethered to a grafting surface with density σ , can be converted in a statistical field theory³⁷, according to the general formulation of model F and model K , as defined in the classical inhomogeneous polymer system classification³⁸. After integrating out the solvent degrees of freedom, and considering the case of strong polyelectrolytes, so that the polymer charge distribution is independent on the location of each monomer and smeared along the chain with a uniform charge ratio f , the effective hamiltonian of the system reads

$$\beta\mathcal{H}[w_p, \psi] = \frac{1}{2} \int d\mathbf{r} \left[\frac{1}{v} w_p(\mathbf{r})^2 + \frac{1}{4\pi l_B} |\nabla\psi(\mathbf{r})|^2 \right] - \sigma \int d\mathbf{r}_\perp \ln \mathcal{Q}_p(\mathbf{r}_\perp, i w_p + i z_p \psi) - n_c \ln \mathcal{Q}_c(i\psi), \quad (3)$$

where $w_p(\mathbf{r})$ and $\psi(\mathbf{r})$ are the two fields related to monomer concentration and electrostatic potential, where \mathcal{Q}_p and \mathcal{Q}_c are the single-chain and counter-ion partition functions, defined and in Appendix A and where a uniform distribution for the grafting points is assumed. The excluded-volume parameter, also introduced in Appendix A, represents the effective interaction between monomers. As both the electrostatic and monomer density fields are uniform in the x and y directions, parallel to the grafting surface³⁹, the single-chain polymer energy contribution, along the direction perpendicular to the grafting surface reads

$$\frac{E[z^\alpha; 0, s]}{k_B T} = \int_0^s \left[\frac{3}{2a^2 N} |z^\alpha(t)|^2 + w_p(z^\alpha(t)) \right] dt. \quad (4)$$

The grafting density σ can be absorbed introducing rescaled polymer and counter-ion concentrations,

$$\phi_p(z) = \frac{a\rho_0}{\sigma N^{1/2}} \langle \hat{\phi}_p(z) \rangle \quad (5)$$

and

$$\phi_c(z) = \frac{a\rho_0}{f\sigma N^{1/2}} \langle \hat{\phi}_c(z) \rangle, \quad (6)$$

that are now normalized according to

$$\int_0^d \phi_p(z) dz = aN^{1/2} \quad (7)$$

$$\int_0^d \phi_c(z) dz = aN^{1/2}. \quad (8)$$

The corresponding field equations are

$$\begin{aligned} w_p(z) &= \Lambda \phi_p(z) + N_c \psi(z) \\ w_c(z) &= -N \psi(z), \end{aligned} \quad (9)$$

where the reduced interaction parameter is defined as⁴⁰,

$$\Lambda \equiv \frac{v\sigma N^{3/2}}{a\rho_0}, \quad (10)$$

and is related to the brush height L according⁴¹ to $L/aN^{1/2} = (4\Lambda/\pi^2)^{1/3}$, where we introduce the number of ions per polymer parameter $N_c = fN$, and where all length scales are expressed in units of $aN^{1/2}$.

III. SELF-CONSISTENT FIELD THEORY

The crux of self-consistent field theory is the one-dimensional polymer partition function,

$$\begin{aligned} q(z, z_0, s) &= \int \mathcal{D}z_\alpha \exp\left(-\frac{E[z^\alpha; 0, s]}{k_B T}\right) \\ &\times \delta(z_\alpha(s) - z) \delta(z^\alpha(0) - z_0), \end{aligned} \quad (11)$$

for a section of sN segments with its ends at $z^\alpha(0) = z_0$ and $z^\alpha(s) = z$. The polymer partition function satisfies the modified diffusion equation¹¹

$$\frac{\partial}{\partial s} q(z, z_0, s) = \left[\frac{a^2 N}{6} \frac{\partial^2}{\partial z^2} - w_p(z) \right] q(z, z_0, s) \quad (12)$$

where $q(z, z_0, 0) = aN^{1/2} \delta(z - z_0)$ and $q(0, z_0, s) = 0$, and where the field equations (9) include a contribution from the dimensionless electrostatic potential $\psi(z)$, that satisfies a non-linear Poisson-Boltzmann equation

$$\frac{1}{L_B} \frac{\partial^2}{\partial z^2} \psi(z) = \phi_c(z) - \phi_p(z), \quad (13)$$

with boundary conditions

$$\begin{aligned} \Lambda_{GC} \frac{\partial}{\partial z} \psi(z) \Big|_{z=0} &= -1 \\ \Lambda_{GC} \frac{\partial}{\partial z} \psi(z) \Big|_{z=d} &= +1, \end{aligned} \quad (14)$$

that describe an external surface charge, where

$$L_B \equiv [(ze)^2 / \varepsilon a N^{1/2} k_b T] / \sigma N_c \quad (15)$$

is the rescaled Bjerrum length parameter and where the Gouy-Chapman length is defined as

$$\Lambda_{GC} \equiv z f \sigma N / \Sigma L_B. \quad (16)$$

The counter-ion distribution is given by

$$\phi_c(z) = \frac{aN^{1/2}}{\mathcal{Q}_c} \exp(-w_c(z)/N), \quad (17)$$

where

$$\mathcal{Q}_c = \int_0^d \exp(-w_c(z)/N) dz. \quad (18)$$

Once the solution $q(z, z_0, s)$ to the modified diffusion equation (12) has been found, the concentration profile for a chain with its free-end at $z = z_0$ can be computed according to

$$\phi_p(z; z_0) = \int_0^1 \frac{q(\epsilon, z, 1-s) q(z, z_0, s)}{q(\epsilon, z_0, 1)} ds, \quad (19)$$

where ϵ is a small finite distance from the grafting surface introduced according³⁹ to the standard formulation of model K . The free-end distribution is defined as

$$g(z_0) = \frac{aN^{1/2}}{\mathcal{Q}_P} \exp\left(-\frac{f_0(z_0)}{k_B T}\right), \quad (20)$$

where

$$f_0(z_0) = -\ln q(0, z_0, 1) \quad (21)$$

and where finally

$$\mathcal{Q}_P = \int_0^d \exp\left(-\frac{f_0(z_0)}{k_B T}\right) dz_0, \quad (22)$$

and the monomer density distribution satisfies

$$\phi_p(z) = \frac{1}{aN^{1/2}} \int_0^d g(z_0) \phi_p(z; z_0) dz_0. \quad (23)$$

The set of self-consistent field equations (12)-(13) have been solved numerically, for different values of the four fundamental parameters, namely the natural brush height $L/aN^{1/2}$, the number of ions per polymer $N_c \equiv fN$, the rescaled Bjerrum Length L_B and the relative surface charge parameter

$$f_e = \Sigma / z f \sigma N, \quad (24)$$

where Σ is the total charge on the grafting surface in elementary charge units. The free-energy of the system can be computed as

$$\begin{aligned} \frac{F}{k_B T n_c} &= \frac{1}{aN^{1/2} N_c} \int_0^d g(z_0) \left[\frac{f_e(z_0)}{k_B T} + \ln g(z_0) \right] dz_0 \\ &+ \frac{1}{aN^{1/2}} \int_0^d dz \phi_c(z) \ln \phi_c(z) dz + \frac{\Lambda}{2aN^{1/2} N_c} \int \phi_p^2(z) dz \\ &+ \frac{1}{2aN^{1/2}} \int_0^d \psi(z) [\phi_p(z) - \phi_c(z)] dz, \end{aligned} \quad (25)$$

where the first term is the polymer free-energy and is obtained as the sum of the translational entropy of the chain ends and the average of the stretching energy

$$\frac{f_e(z_0)}{k_B T} = -\ln q(\epsilon, z_0, 1) - \frac{1}{aN^{1/2}} \int w(z)\phi(z, z_0)dz, \quad (26)$$

the second term represents the translational entropy of the mobile counter-ions and the third and fourth terms the interaction energy, due to excluded-volume interactions between polymer segments and the electrostatic energy related to the charge distribution in the system respectively. Details on the derivation of equation (25) can be found in Appendix B.

IV. STRONG-STRETCHING THEORY

When the polymer chains are stretched it is possible to exploit the analogy between polymer field theory and quantum mechanics and approximate the single-chain partition function in equation (11), defined above within the path-integral formalism, by considering the dominant contribution of the classical path and the fluctuations around it^{42,43}. The problem in this limit relates to the classical mechanics problem of a particle moving down an incline¹⁴. In the classical limit, the partition function $q(0, z_0, 1)$ is dominated by the path $z_\alpha(s)$ that minimizes the energy in equation (4) and an estimate for the free-energy $f_0(z_0)$ of a chain extending to $z = z_0$, can be obtained accordingly:

$$q(0, Z_0, 1) \propto \exp\left(-E[Z^\alpha; 1]/k_B T\right), \quad (27)$$

where, from here on, we will use dimensionless units $Z = z/aN^{1/2}$. Following the general principle of strong-stretching theory^{42,44} we write,

$$\frac{3}{2}S^2(Z, Z_0) \equiv N_c \left[\frac{3}{2}v^2(Z_0) + U(Z) - U(Z_0) \right], \quad (28)$$

where the potential $U(Z)$ is to be identified with the polymer field $w_p(z)$ introduced in equation (9). The chain-end tension can be written⁴³ as

$$v(Z_0) = -\frac{d \ln g(Z_0)}{dZ_0}, \quad (29)$$

and, in dimensionless units, the two constraints

$$\int_0^{Z_0} \frac{1}{S(Z, Z_0)} dZ = 1, \quad (30)$$

and

$$\int_Z^D \frac{g(Z_0)}{S(Z, Z_0)} dZ_0 = \phi_p(Z), \quad (31)$$

apply. This yields an expression for the dimensionless speed at position Z , $S(Z, Z_0)$ and the normalization condition in equation (30), corresponding to the

isochronicity constraint for the effective particle rolling down an incline⁴⁰. In the absence of excluded-volume interactions^{35,44}, the normalization condition in equation (30) can be written as an Abel-Volterra integral equation of the first kind⁴⁵. Its solution leads to a parabolic form for the potential $U(Z)$ ^{42,46}. Neglecting the term related to the end-monomer tension, i.e. setting $v(Z_0) \approx 0$, one finds the integral equation

$$\int_U^{U_0} dt f(t)(t - U)^{-1/2} = 1, \quad (32)$$

and its solution, in terms of the Riemann-Liouville fractional derivative of order $1/2$, as discussed in Appendix C, reads

$$f(U) = \sqrt{\frac{3}{2}} \frac{dZ}{dU} = -\frac{1}{\pi} \frac{d}{dU} \int_U^{U_0} dt (t - U)^{-1/2}. \quad (33)$$

The associated potential form is obtained as

$$U(Z) = \frac{3\pi^2}{8}(H^2 - Z^2), \quad (34)$$

and the electrostatic potential $\psi^a(Z) = N_c^{-1/2}U(Z)$ follows a parabolic form, according to strong-stretching theory⁴⁴. We express distances in dimensionless rescaled units $Z' = Z/N_c^{1/2}$, where H represents the brush height in units of Z . The relative charge ratio per chain reads $Q_1 = 1 - \frac{H}{\gamma}$, where

$$\gamma = \frac{4}{3\pi^2} L_B N_c^{3/2}. \quad (35)$$

The rescaled counter-ion distribution is given by

$$N_c^{1/2} \phi_c^a(Z) = \frac{3\pi^2 H^2}{8\gamma} \exp\{\psi^a(Z)\}, \quad (36)$$

and the electrostatic potential outside the brush is written as

$$\psi^b(Z) = -2 \ln \left(\gamma^{1/2} (Z - H + 1/H) \right), \quad (37)$$

where the brush height⁴⁴ is given by

$$H + \frac{\sqrt{\pi}}{2} \sqrt{\frac{3\pi^2}{8}} H^2 e^{\frac{3\pi^2}{8} H^2} \operatorname{erf} \left(\sqrt{\frac{3\pi^2}{8}} H \right) = \gamma, \quad (38)$$

the monomer density distribution,

$$N_c^{1/2} \phi_p(Z) = N_c^{1/2} \phi_c^a(Z) + 1/\gamma, \quad (39)$$

and the counter-ion distribution outside the brush is given by the Gouy-Chapman form,

$$\phi_c^b(Z) = \frac{1}{\gamma} (Z - H + 1/H)^{-2}. \quad (40)$$

The size of the brush can be expressed as

$$\frac{\langle Z \rangle}{H} = \frac{H^2}{2\gamma} e^{\frac{3\pi^2}{8} H^2}. \quad (41)$$

Finally the end-monomer distribution can be obtained, as detailed in the Appendix C, solving⁴⁴ a similar Abel-Volterra equation of the first kind to equation (30), that corresponds to the constraint of equation (31). One finds,

$$\begin{aligned} \gamma N_c^{1/2} g(Z) &= \sqrt{\frac{3\pi^2}{8}} Z \left(1 + \frac{3\pi^2 H^2}{8}\right) (\psi^a(Z))^{-1/2} \\ &+ \sqrt{\pi} \frac{3\pi^2}{8} H^2 \exp(\psi^a(Z)) \operatorname{erf}(\sqrt{\psi^a(Z)}). \end{aligned} \quad (42)$$

In the following section we will compare the strong-stretching theory predictions with the results obtained within self-consistent field theory, where the Poisson-Boltzmann and modified diffusion equations (12)-(13) are solved explicitly by finite difference methods. We consider both the case of excluded-volume and electrostatic interactions being present. It is important to note at this point that typical synthetic polymers considered in experimental conditions are relatively insensitive to solvent conditions and the long range electrostatic interactions will dominate in some cases³⁵.

V. SELF-CONSISTENT FIELD THEORY-RESULTS

In the previous section we discussed the main assumptions and results of strong-stretching theory and introduced the fundamental equations for the monomer density and electrostatic potential in a system of uniformly charged polyelectrolyte chains, tethered to a flat interface, in the absence of the external field. The numerical method, used to solve the mean-field saddle point equations discussed within self-consistent field theory, is introduced in this section and the results throughout discussed and compared with the analytical predictions of strong-stretching theory⁴⁴. In order to solve the coupled set of saddle-point equations (12)-(13), we used a real-space, finite difference second-order method⁴⁷. The modified diffusion equation (12) was solved using a discrete Crank-Nicholson real-space method, as discussed in detail in the past⁴⁰. The full Poisson-Boltzmann equation (13) was solved using an iterative Newton-Raphson method, where the partition function for the small species is calculated at each iteration step. The algorithm we implemented in order to solve the modified diffusion equation (12) includes the Anderson mixing method⁴⁸. We observe our algorithm to converge efficiently in a broad range of parameter values. It is important to mention that we observe the range of convergence, namely the highest number of ions per chain the algorithm can reach for a given value of the Bjerrum length and brush thickness parameters, to depend in a non trivial way on the Anderson mixing method. Avoiding the Anderson mixing method and decreasing the mixing parameter μ to very small values, typically $\mu = 0.01$, improves the range of convergence but increases the time of convergence significantly. A typical threshold value we obtained and

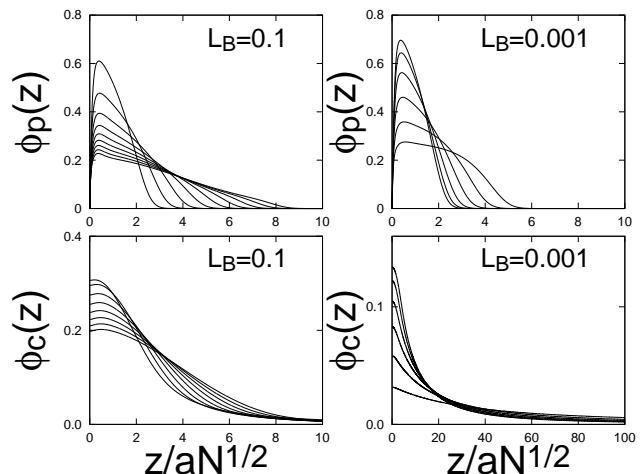


FIG. 1. The two upper plots represent the monomer density profile for the value of the brush thickness $L/aN^{1/2} = 2$ and for increasing values of the number of ions per chain $N_c = 10 \dots 90$ and $N_c = 30, 60, \dots 180$, for the values of the Bjerrum Length parameter $L_B = 0.1$ and $L_B = 0.001$ respectively. The two lower plots represent the corresponding counter-ion concentration profiles for $N_c = 20 \dots 100$, $N_c = 30, 60, \dots, 180$.

report for comparison: $N_c^{max} \simeq 200$, for values of $L = 2$ and $L_B = 0.1$ of the brush thickness and Bjerrum length parameters respectively.

A first set of numerical results has been obtained for values of the brush thickness parameter $L = 2$ and Bjerrum length values $L_B = 0.1$ and $L_B = 0.003$. The results for the monomer density and counter-ion distributions, for increasing ionic strength $N_c = 10, \dots, 100$ and $N_c = 30, \dots 180$ for two different values of the Bjerrum length parameter $L_B = 0.1$ and $L_B = 0.001$ are shown in Fig 1. Another set of calculations have been performed at the values of $L \simeq 1.88$, $L_B \simeq 0.68$ to confirm the agreement with closely related calculations³³. We note that, when exceeding the values of the number of ions per chain $N_c = 30$, considered in that paper as a limiting threshold, a peak at low values of the distance appears, already discussed⁴⁹. Our findings resolve the inconsistency reported³³ for the monomer density profiles at small values of the grafting distance $z/aN^{1/2} \simeq 0.05$, where a peak, as can be seen by close inspection of Fig. 1 appears. The presence of this peak has already been reported⁴⁹ when considering high values of the ion-per-chain parameter $N_c > 50$.

All calculations of this and the following sections were performed considering value of the rescaled distance $D = d/aN^{1/2}$ between the grafting surface and the electrode to be large enough, so to measure a vanishing counter-ion density at the boundaries. In order to obtain such condition, at the lowest values of the Bjerrum length parameter considered, e.g. $L_B = 0.0003$, we needed to consider values of order $D = 10^3$. This was possible as the two grids we consider to solve the modified diffusion

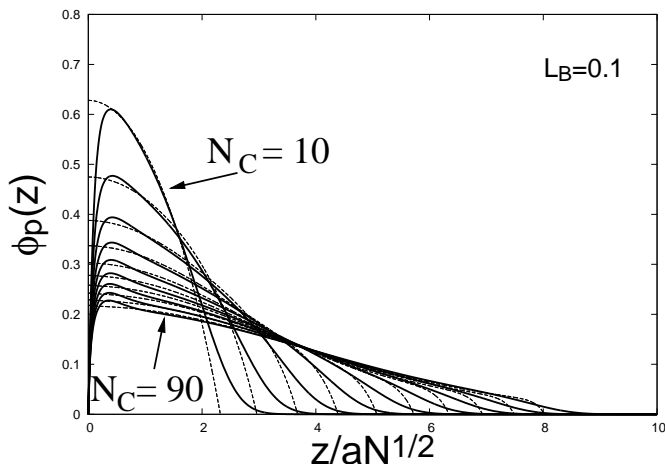


FIG. 2. Solid lines represent the self-consistent field theory results for the monomer concentration profiles for values of the brush thickness parameter $L/aN^{1/2} = 2$ and Bjerrum length $L_B = 0.1$, for increasing values of the ion number parameter $N_c = 10, \dots, 90$. The dashed lines are the results obtained with the numerical strong-stretching approach discussed in the text.

equation (12) and equation (13) did not have the same size, the second grid exceeding the size of the first, depending on the Bjerrum length values considered. This can be seen looking at the range of distances $z/aN^{1/2}$ we plot in Fig. 1 for different values of the Bjerrum length parameter L_B .

Another method introduced in the past to avoid the numerical self-consistent field theory approach is to linearize³⁰ the Poisson-Boltzmann equation (13) and to modify the strong-stretching theory accordingly. As a third, intermediate option, we considered explicitly the Poisson-Boltzmann equation (13) and combined its numerical solution with the analytical form of the potential, as predicted by strong-stretching theory. We hence assume a parabolic form for the effective potential $w(Z)$ and solve numerically the Poisson-Boltzmann equation (13), and an estimate for the monomer concentration profile, together with the electrostatic potential, follows directly. The procedure is iterated until convergence is achieved. A comparison with the results obtained by the full solution of equations (12) and (13) is shown in Fig. 3. Closely related methods and results have also been discussed³¹.

We now consider the case where excluded-volume interactions are neglected³⁵. The validity of this assumption⁴⁴ is tested and comparison between polyelectrolyte scaling and strong-stretching theory and the numerical results obtained within self-consistent field theory, when solving the saddle point equations (12)-(13) is presented. We assume here the relative strength of the excluded-volume interactions to be small with respect to the average electrostatic interaction strength, so that the solvent can be considered as a θ solvent for uncharged

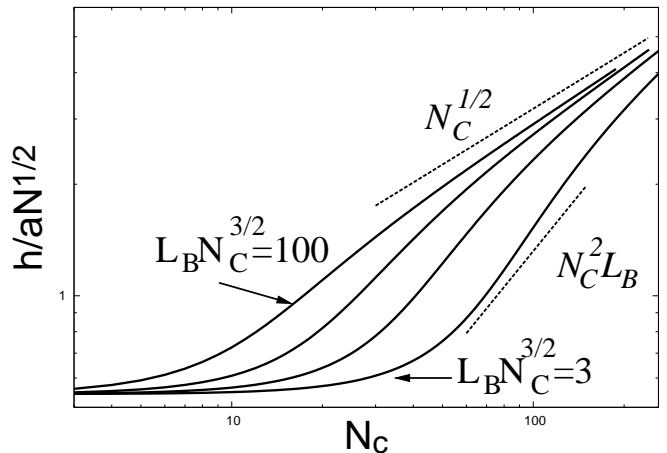


FIG. 3. Brush thickness $h/aN^{1/2}$ as a function of the number of ions per chain N_c , for different values of the Bjerrum length $L_B = 0.003, 0.01, 0.03, 0.1$, neglecting excluded-volume interactions. The two dotted lines are the scaling predictions corresponding to the osmotic and Pincus regimes²⁹ respectively.

chains. This assumption, already discussed and justified in detail³⁵, will be considered in the results of Figs. 3- 6, so to compare with scaling and strong-stretching theory.

In Fig. 3 we present the results for the brush thickness $h/aN^{1/2}$, as obtained from the first moment of the monomer concentration profile, for increasing values of the number of ions per chain parameter N_c and for vanishing values of $L/aN^{1/2}$. The classical scaling predictions, discussed in the literature²⁹, are clearly confirmed, given in particular the large values of the number of ions per chain parameter our algorithm was capable to achieve. The data fit the asymptotic behavior expected at large values of the number of ions per chain parameter N_c , as shown by the upper dotted line of Fig. 3, where the condition of static equilibration of the osmotic pressure dictates²⁹, in the strongly charged regime, the scaling law $h/aN^{1/2} = N_c^{1/2}$. According to the results presented in Fig. 3, an intermediate cross-over regime, the so-called Pincus-regime²⁹, is present. The curves, corresponding to different values of the Bjerrum length parameter $L_B = 0.003, 0.01, 0.03, 0.1$, cross-over to the intermediate scaling regime, according²⁹ to the scaling expression $h/aN^{1/2} = N_c^2 L_B$, corresponding to the slope of the second dashed line in Fig. 3. The region for this crossover to occur is quite narrow: all curves in Fig. 3 converge to the neutral brush thickness¹³ value $h_o/aN^{1/2} \simeq 0.54281$, thus explaining why evidence of the Pincus regime in numerical simulations turns out to be an elusive task⁵⁰. In Fig. 4 we compare the numerical results obtained by the numerical self-consistent field theory with the predictions of strong-stretching theory, as described by equation (39), for the four values of the strong-stretching parameter $L_B N_c^{3/2} = 3, 10, 30, 100$. At large values of γ the agreement between the numerical results and the theory

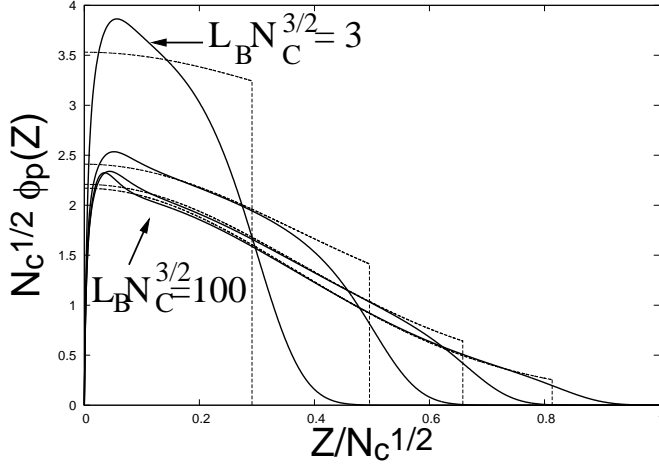


FIG. 4. Monomer concentration profile as a function of rescaled distance from the grafting surface $Z/aN_c^{1/2}$, for different values of the strong-stretching parameter $L_B N_c^{3/2} = 3, 10, 30, 100$. Solid lines are the results obtained with self-consistent field theory. The dashed lines are the predictions of strong-stretching theory. Agreement between strong-stretching and the self-consistent field theory becomes very good for large values of the parameter γ .

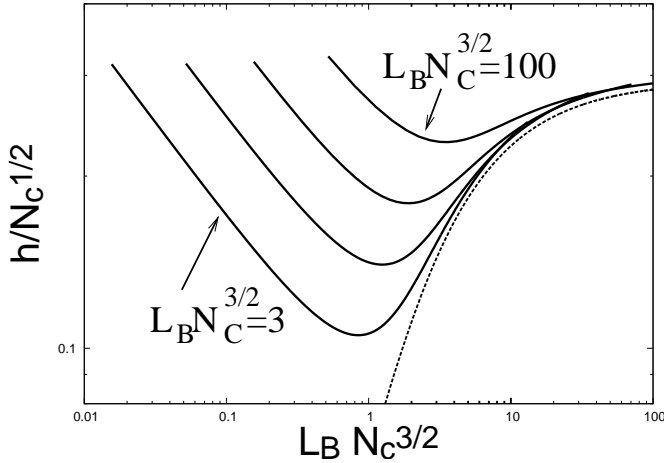


FIG. 5. Brush thickness as obtained from the first moment of the monomer concentration profile predicted by self-consistent field theory (solid-lines), for four different values of the Bjerrum length $L_B = 0.0003, 0.001, 0.003, 0.1$ and the prediction of strong-stretching theory in equation (41) as a function of the strong-stretching parameter γ . The agreement becomes very good at large values of γ . A small discrepancy though is observed. The reason for this discrepancy is not clear.

becomes very good, except at small values of the rescaled distance $Z/N_c^{1/2} < 0.05$, and at the edge of the brush, as expected.

A few conclusive remarks, while closing this section, are here in order. As shown in Fig. 6, the fundamental assumption of strong-stretching theory becomes more accu-

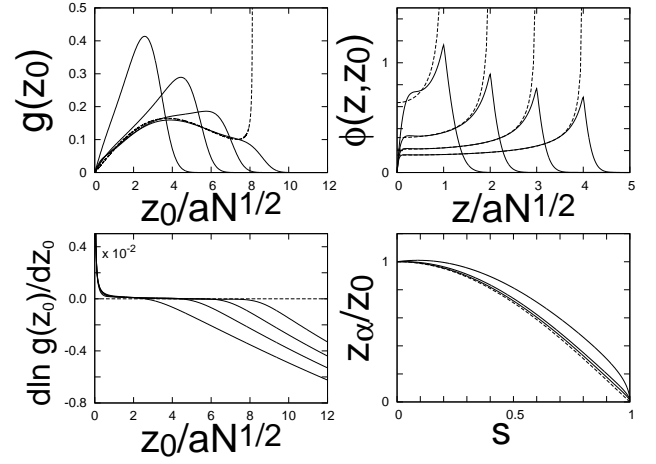


FIG. 6. The left upper plot represents the end-segment distribution $g(z_0)$. The solid curve corresponds to the results obtained within self-consistent field theory, at values of the strong-stretching parameter $L_B N_c^{3/2} = 3, 10, 30, 100$. The dashed line corresponds to the prediction of equation (42) for $L_B N_c^{3/2} = 100$. The agreement is good for all values of the distance from the grafting surface $z/aN^{1/2}$, except at large values where the prediction of equation (42) diverges. In the lower left plot we show the chain-end tension for the four values of the strong-stretching parameter above. The upper right plot shows the segment profiles $\phi(z, z_0)$ for $L_B N_c^{3/2} = 100$ for the four values of the end position $z_0/aN^{1/2} = 1, 2, 3, 4$. The corresponding prediction of strong-stretching theory is represented by the dashed lines. The corresponding average polymer trajectories are shown in the lower right plot together with the prediction of strong-stretching theory, shown by the dashed line.

rate for increasing values of the strong-stretching parameter $L_B N_c^{3/2}$. At values of $L_B N_c^{3/2} = 100$, the chain-end tension, as measured within self-consistent field theory, approaches zero, for all values of the distance $z/aN^{1/2}$ inside the brush. Fig. 6 also shows the segment profiles $\phi(z, z_0)$, for chains with different end-positions z_0 at values of $L_B N_c^{3/2} = 100$ and the corresponding average polymer trajectories $z_\alpha(s)/z_0$ as obtained within self-consistent field theory, together with the prediction of strong-stretching theory. We finally present the results obtained within self-consistent field theory, when considering a uniform charge on the grafting surface. We obtained results for both the case of similarly and oppositely charged surface. The monomer-density and counter-ion distribution profiles are shown in Fig. 7 and Fig. 8.

The results were obtained for both positive and negative values of the relative surface charge parameter f_e , for a brush thickness parameter value $L/aN^{1/2} = 2$. The boundary condition in equation (14) has been changed accordingly. As expected, for the case of a similarly charged surface, the polymer brush swells, and the monomer-density profile obtained at small values of the relative surface charge parameter changes its shape

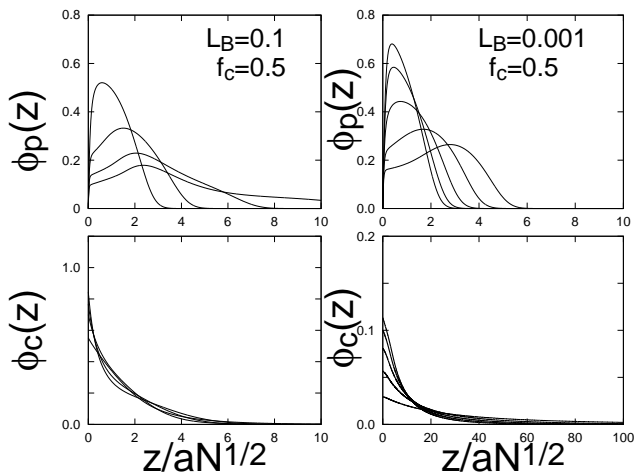


FIG. 7. Monomer concentration $\phi_p(z)$ and counter-ion distribution profiles $\phi_c(z)$, for brush thickness values of $L/aN^{1/2} = 2$ and for two values of the Bjerrum length parameter $L_B = 0.1$ and $L_B = 0.001$, as a function of the distance from the grafting surface, for positive values of the relative surface charge parameter $f_e = 0.5$, for increasing values of the number of ions per chain parameter $N_c = 10, \dots, 40$ and $N_c = 30, 60, \dots, 150$ respectively.

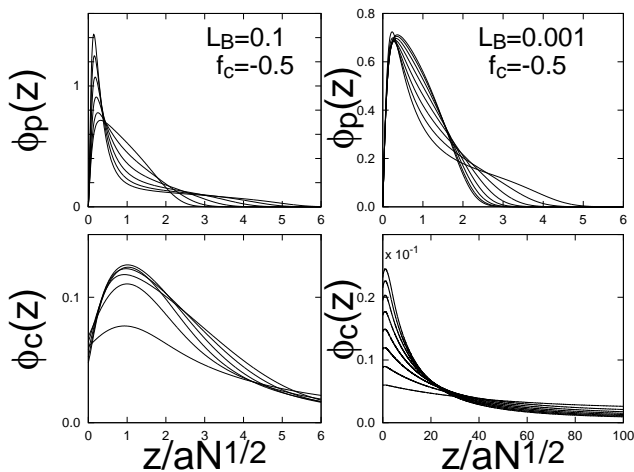


FIG. 8. Monomer concentration $\phi_p(z)$ and counter-ion distribution profiles $\phi_c(z)$, for brush thickness values of $L/aN^{1/2} = 2$ and for two values of the Bjerrum length parameter $L_B = 0.1$ and $L_B = 0.001$, as a function of the distance from the grafting surface, for negative values of the relative surface charge parameter $f_e = -0.5$ and for increasing values of the number of ions per chain parameter $N_c = 10, \dots, 60$ and $N_c = 30, 60, \dots, 240$ respectively.

and deviates from the parabolic form. Similarly, when considering an oppositely charged grafting surface, as in Fig. 8, the brush contracts and the counter-ion distribution changes self-consistently. Related results, for the case of a similarly charged grafting surface, have been reported in the past³⁵.

VI. CHARGED-END-GROUP POLYMER BRUSHES

In the previous section we presented numerical self-consistent field theory results for uniformly charged, end-grafted polyelectrolyte systems, both in the presence and in the absence of excluded-volume interactions and discussed the effects of a uniform electric field. We discussed the results for the chain-end, counter-ion and monomer-density distributions, for different values of the relative surface charge parameter f_e . The analysis suggested that the parabolic form of the monomer density profile is drastically affected by the electric field, both in the similarly and the oppositely charged case.

We consider in this section the case of a polymer brush in solution, characterized by charged end-groups^{22,23} in the presence of counter-ions and excluded-volume interactions between the monomers. Rather than considering a uniformly charged polyelectrolyte, as discussed in section V, we study in this section the case of grafted neutral chains, with a functional charged end-group, represented in our model by the terminal, non-grafted χN monomers along the chain. As discussed above, we consider the case of strong polyelectrolytic functional groups, so that the charges are assumed to stay bounded to the chain-ends. As for the case of uniformly charged polyelectrolytes, the N_c ions per chain are uniformly smeared along the terminal, non-grafted section of the chain, with a rescaled charge density f/χ so that, consistently with the notation of Appendix A, we consider the charge distribution along the chains to be given by $z_p(s) = f/\chi\Theta(s-\chi)$. We solve the saddle-point equations (12)-(13) that now involve both the charged and uncharged monomer densities and the effective field $w_p(z)$ is also defined accordingly. In Fig. 9 we show the total (charged and uncharged) monomer density distribution of a brush of thickness $L/aN^{1/2} = 4$, for increasing values of the number of ions per chain-end parameter $N_c = 1, 10, 20$. For small values of the ions per chain parameter, namely $N_c = 1$, the electrostatic interactions between the chain-ends are negligible, as can be seen in Fig. 9 and the monomer distribution is close to the parabolic prediction of strong-stretching theory, the brush thickness parameter $L/aN^{1/2}$ being relatively large, as expected. Deviations from the parabolic profiles can be observed and are due to the inter-chain-end electrostatic interactions at higher values of the ion-per-chain-end parameter N_c . The calculation has been performed for the specific value of $\chi = 1/30$, so that the size of the polymer chain is about thirty times the size of the chain-end group. We performed several test runs and checked that for smaller sizes of the chain-end group the monomer density profiles did not change significantly. For increasing values of N_c the brush swells, due to the repulsive electrostatic chain-end interactions and the counter-ion distribution changes accordingly. We now discuss the response of the system to an electric field. In our analysis we consider small values of the number of ions per chain-end parameter, namely $N_c = 1$, so to minimize the interaction between the chain-ends.

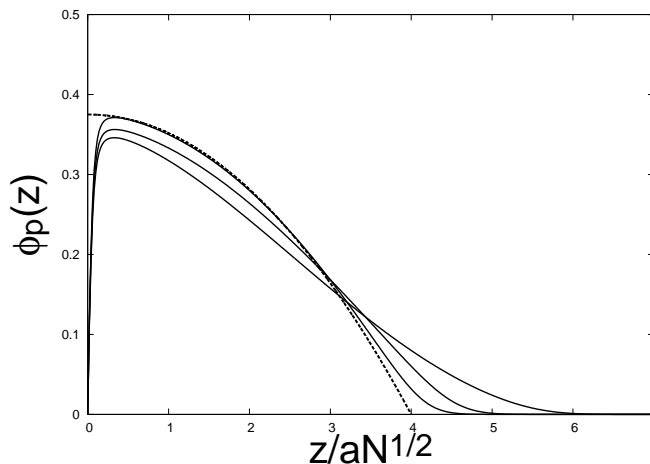


FIG. 9. Monomer density profiles for a brush with thickness parameter $L/aN^{1/2} = 4$, Bjerrum length parameter value $L_B = 0.1$ for increasing values of the number of ion-per-chain-end parameter $N_c = 1, 10, 20$. The dashed line represents the prediction of strong-stretching theory, in the absence of charged-end-groups.

As discussed in section IV, we consider the brush to be grafted to a flat surface that acts as an electrode, while the second electrode is kept at a distance $D \gg L$. In order to study the response of the system to the uniform electric field, we solved the saddle point equations (12) and (13) changing the boundary conditions for the electrostatic potential as well as modifying the effective field accordingly. Fig. 11 shows the monomer density profiles for the brush of thickness $L/aN^{1/2} = 4$, Bjerrum length $L_B = 0.1$ and number of ions per chain-end parameter $N_c = 1$ for both positive and negative values of the surface charge $f_e L_B = \pm 2$. The neutral surface charge case $f_e = 0$ is also shown. As expected, we observe deviations from the parabolic profile for finite values of the electric field strength. Differently, for vanishing values of the surface charge $f_e = 0$, the profile is very close to the strong-stretching parabolic prediction, the value of the brush thickness $L/aN^{1/2} = 4$ being relatively large⁴⁰. In the following section we discuss how to generalize strong-stretching theory for the case of a uniform electric field, assuming the relative charge at the chain-ends to be small.

VII. STRONG-STRETCHING THEORY OF CHARGE-END-GROUP POLYMER BRUSHES

The mathematical foundations of strong-stretching theory stem from the fact that the isochronicity constraint in equation (30) may be regarded as an Abel-Volterra integral equation of the first kind. This determines uniquely the form of the potential⁴². To determine how a uniform tension at the chain-ends, induced by the electric field, affects the potential form $U(Z)$,

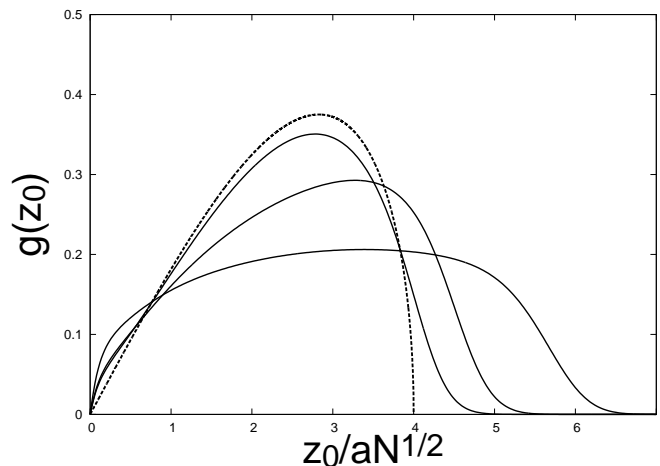


FIG. 10. Chain-end distribution $g(z_0)$ for a brush with thickness parameter $L/aN^{1/2} = 4$, Bjerrum length parameter value $L_B = 0.1$ for increasing values of the number of ion-per-chain-end parameter $N_c = 1, 10, 20$. The dashed line represents the prediction of strong-stretching theory, in the absence of charged-end-groups.

we evaluated the corresponding corrections, solving the isochronicity constraint condition in equation (30). The presence of the electric field induces a chain-end uniform tension and converts the associated integral equation from an Abel-Volterra equation of the first kind to an Abel-Volterra equation of the second kind, as also discussed in detail in Appendix C. This leads to evaluate the main corrections to the parabolic potential, due to the presence of the field, as we now derive. Let us consider directly the constraint in equation (30), that can be written, following the few steps in Appendix C,

$$\int_{\eta}^{U_0} dt (t-\eta)^{-1/2} = \int_{\eta}^{U_0} dt f(t) \left\{ \pi - \alpha (t-\eta)^{-1/2} \right\}, \quad (43)$$

where $f(U) = \sqrt{\frac{3}{2}} \frac{dZ}{dU}$ is related to the first derivative of the inverse function $Z(U)$. We then find corrections to the strong-stretching results. Namely, after a few steps, we obtain the following Abel-Volterra integral equation of the second kind:

$$\frac{df(\eta)}{d\eta} - \frac{\pi}{\alpha^2} f(\eta) = \frac{d}{d\eta} F(\eta)$$

$$F(\eta) = g(\eta) - \frac{1}{\alpha} \int_{\eta}^{U_0} dt g(\eta) (t-\eta)^{-1/2}, \quad (44)$$

where $g(\eta) = -1/\alpha$, and where $\alpha = \sqrt{6}V_0$ measures the uniform end-monomer force induced by the electric field at the chain ends. The solution to this Abel-Volterra integral equation of the second kind can be obtained as follows:

$$f(\eta) = \frac{dZ}{d\eta} = \frac{1}{\alpha} e^{\frac{\pi}{\alpha^2}(U_0-\eta)} \frac{1}{\sqrt{\pi}} \Gamma\left(\frac{1}{2}, \frac{\pi}{\alpha^2}(U_0-\eta)\right), \quad (45)$$

$\Gamma(\alpha, x)$ being the incomplete gamma function of order α . The above expression can be integrated and the corresponding equation for the potential reads

$$\sqrt{\frac{3}{2}}Z = \frac{2}{\pi}(U_0 - U)^{1/2} + \alpha - \frac{\alpha}{\sqrt{\pi}} e^{\frac{\pi}{\alpha^2}(U_0 - \eta)} \Gamma\left(\frac{1}{2}, \frac{\pi}{\alpha^2}(U_0 - \eta)\right). \quad (46)$$

The expression above reduces to the parabolic strong-stretching potential when the chain-end tension vanishes, as expected. From the potential in equation (46), we determined the monomer-density and chain-end distributions by means of the field equation (9), in the limit of weakly charged end-groups. This assumption has been justified and discussed in Fig. 10. A similar analysis, detailed in Appendix C, leads to an explicit expression for the chain-end distribution $g(Z_0)$, for small values of the electric field strength α . We find, after a few steps detailed in Appendix C,

$$g(\eta) \frac{dZ}{d\eta} = -\frac{2}{\pi} \eta^{1/2} + \frac{\alpha}{2} - \frac{\alpha}{\pi^{3/2}} e^{\frac{\pi}{\alpha^2} \eta} \Gamma\left(\frac{1}{2}, \frac{\pi}{\alpha^2} \eta\right). \quad (47)$$

Equation (47) reduces to the well known expression for the chain-end distribution⁴², when no tension is present at the chain-ends. The value of the chain-end prefactor $\delta \simeq 0.263$ has been obtained comparing the results of numerical self-consistent field theory, as in the inset of Fig. 12, and the results obtained from equation (46) for the brush height $h/aN^{1/2}$. It would be interesting to see if the prefactor can be computed explicitly, and if it depends on the brush thickness parameter $L/aN^{1/2}$.

Equations (46) and (47) generalize the MWC strong-stretching theory to problem of charge-end functionalized brushes in the presence of a small, uniform external electric field. A comparison with the results of numerical self-consistent field theory is shown in Fig. 11 and Fig. 12.

We conclude observing that the monomer-density profile is affected by the uniform electric field in a different way that what seen for uniformly charged polyelectrolyte brushes. Note however that, when comparing the results of this section with the monomer-density profiles of Fig. 7 and Fig. 8 one should keep in mind that the results discussed for the polyelectrolyte problem were obtained at relatively large values of the number of ions per chain parameter N_c , the electrostatic interactions between monomers being relatively strong. It is interesting to observe that for a uniformly charged polyelectrolyte system, at low values of the number of ions per chain parameter, e.g. $N_c = 1$, the effect of the uniform electric field is very similar to what observed for charged-end-group chains and the monomer-depletion effect close to the surface, seen in the analysis of Fig. 7 for a similarly charged surface, is not present, as in the case of grafted charge-end-group polymer chains discussed in this section. This suggests that the strong-stretching theory corrections discussed in this work might apply reasonably well for the problem of weakly charged polyelectrolyte chains in a uniform electric field.

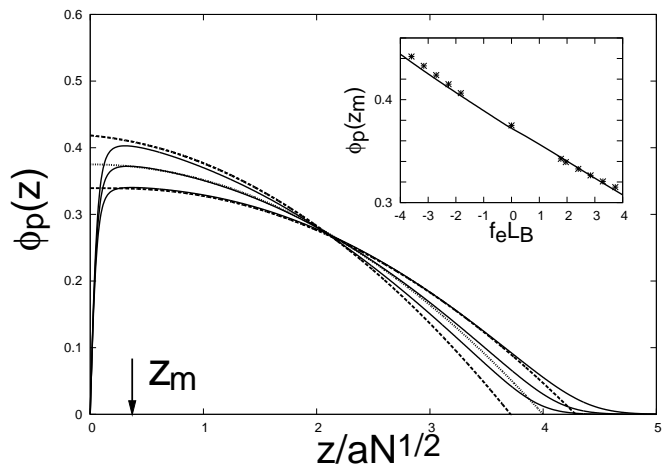


FIG. 11. Monomer density profile $\phi_p(z)$ for a brush with thickness parameter $L/aN^{1/2} = 4$, Bjerrum length parameter value $L_B = 0.1$, for values of the number of ion-per-chain-end parameter $N_c = 1$, for neutral surface charge $f_e = 0$, as well as similarly and oppositely charged grafting surface, with rescaled surface charge parameter values $f_e L_B = \pm 2.0$. The dotted line represents the prediction of strong-stretching theory, in the absence of charged-end-groups. The dashed lines represent the prediction of the modified strong-stretching theory (46), for values of the parameter $\alpha = \delta f_e L_B$. The inset shows the monomer-density at the reference distance $z_m = 0.378$, as measured within self-consistent field theory, shown by the solid line, and as predicted by equation (46), for different values of the chain-end tension parameter α , shown by the star symbols.

VIII. CONCLUSIONS

In this work we studied the properties of charged polymers grafted to a flat interface, in the presence of an external electrical field. Different charge configurations have been discussed. We firstly discussed the properties of polyelectrolyte brushes, where the charges are uniformly distributed along the chains, while counter-ions are in solution and free to diffuse between the grafting surface and the second, oppositely charged electrode. The monomer-density and counter-ion distributions have been obtained by numerical self-consistent field theory and comparison has been made with the analytical strong-stretching theory predictions. The effect of a uniform electric field, both in the oppositely and similarly charged case, has been studied. We considered charge-end-functionalized, grafted polymer chain systems. As for the case of polyelectrolyte brushes, we studied the conformational and electrostatic properties of the brush by means of numerical self-consistent field theory. In the case of weakly charged, end-group-functionalized polymers we have been able to generalize the predictions of strong-stretching theory to the case of a uniform electric field. We have shown how the corrections to the MWC theory for the monomer-density and chain-end distributions can be derived in closed form. The presence of an

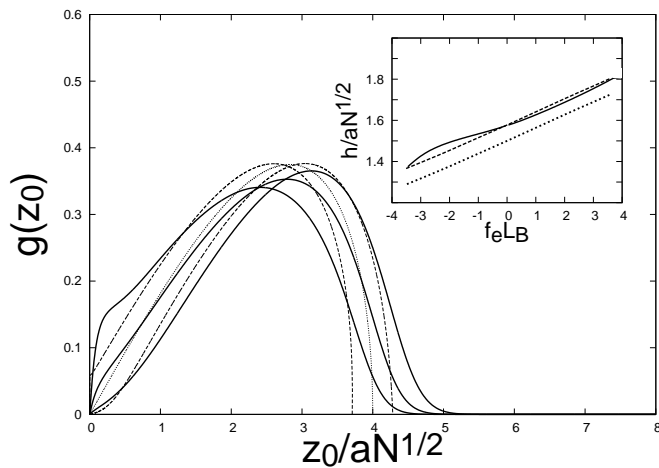


FIG. 12. Chain-end distribution $g(z_0)$ for a brush with thickness parameter $L/aN^{1/2} = 4$, Bjerrum length parameter value $L_B = 0.1$ for values of the number of ion-per-chain-end parameter $N_e = 1$, for neutral surface charge $f_e = 0$, as well as similarly and oppositely charged grafting surface, with rescaled surface charge parameter values $f_e L_B = \pm 2.0$. The dotted line represents the prediction of strong-stretching theory, in the absence of charged-end-groups. The dashed lines represent the prediction of the modified strong-stretching theory in equation (47), for different values of the chain-end tension parameter $\alpha = \delta f_e L_B$. The inset shows the size of the brush $h/aN^{1/2}$, as predicted from numerical self-consistent field theory, shown by the solid line, and as obtained according to the modified strong-stretching theory in equation (46), shown by the dotted line. The dashed line shows the results of the modified strong-stretching theory, shifted by the zero-field value, obtained subtracting the brush size as obtained from self-consistent field theory and the MWC theory prediction.

external field converts the corresponding Abel-Volterra equation from an integral equation of the first kind to an integral equation of the second kind. Deviations from the parabolic profile have been obtained. A comparison of the theory with numerical self-consistent field theory has been performed and agreement has been observed.

ACKNOWLEDGMENTS

This research was funded by EPSRC under grant number EP/F068425/1. I acknowledge very useful discussions with Mark Matsen who participated to the early stages of this work and Jaeup Kim for providing the algorithm that implements the self-consistent field calculation for neutral polymer brushes.

- ¹D. J. Shaw, *Introduction to Colloid and Surface Chemistry* (Butterworth-Heinemann, United Kingdom, 1966).
- ²B. Vincent, *Adv. Colloid Interface Sci.* **4**, 193 (1974).
- ³S. T. Milner, *Science* **251**, 905 (1991).
- ⁴S. Alexander, *J. Phys. (Paris)* **38**, 983 (1977).
- ⁵P. G. de Gennes, *Macromolecules* **13**, 1069 (1980).
- ⁶A. K. Dolan and S. F. Edwards, *Proc. R. Soc. Lond. A* **337**, 509 (1974).

- ⁷A. K. Dolan and S. F. Edwards, *Proc. R. Soc. Lond. A* **343**, 427 (1975).
- ⁸S. F. Edwards, *Proc. Phys. Soc. London* **85**, 613 (1965).
- ⁹E. Helfand, *J. Chem. Phys.* **62**, 999 (1975).
- ¹⁰J. M. H. M. Scheutjens and G. J. Fleer, *Macromolecules* **18**, 1882 (1985).
- ¹¹M. W. Matsen and F. S. Bates, *Macromolecules* **29**, 1091 (1994).
- ¹²H. Orland and M. Schick, *Macromolecules* **29**, 713 (1996).
- ¹³R. R. Netz and M. Schick, *Macromolecules* **31**, 5105 (1998).
- ¹⁴M. W. Matsen, "Self-consistent field theory and its applications," in *Soft Matter*, Vol. 1, edited by G. Gompper and M. Schick (Wiley-VCH Weinheim, 2006) p. 87.
- ¹⁵H. J. Taunton, C. Toprakçioğlu, L. J. Fetters, and J. Klein, *Nature* **332**, 712 (1988).
- ¹⁶C. Singh, G. T. Pickett, E. B. Zhulina, and A. C. Balazs, *J. Phys. Chem. B* **101**, 10614 (1997).
- ¹⁷M. A. Carignano and I. Szleifer, *Interface Sci.* **11**, 187 (2003).
- ¹⁸N.-P. Huang, J. Vörös, S. M. D. Paul, M. Textor, and N. D. Spencer, *Langmuir* **18**, 220 (2002).
- ¹⁹J. Lahann, S. Mitragotri, T.-N. Tran, H. Kaido, J. Sundaram, I. S. Choi, S. Hoffer, G. A. Somorjai, and R. Langer, *Science* **299**, 371 (2003).
- ²⁰P. Gong and I. Szleifer, *Ind. Eng. Chem. Res.* **45**, 5466 (2006).
- ²¹M. A. Carignano and I. Szleifer, *Mol. Phys.* **100**, 2993 (2002).
- ²²V. A. Pryamitsin, F. A. M. Leermakers, and E. B. Zhulina, *Macromolecules* **30**, 584 (1997).
- ²³Y. Tsori, D. Andelman, and J.-F. Joanny, *Europhysics Letters* **82**, 46001 (2008).
- ²⁴H. A. Van der Schee and J. Lyklema, *J. Phys. Chem.* **88**, 6661 (1984).
- ²⁵A.-C. Shi and J. Noolandi, *Macromol. Theory Simul.* **8**, 214 (1999).
- ²⁶I. Borukhov, D. Andelman, and H. Orland, *Eur. Phys. J. B* **5**, 869 (1998).
- ²⁷Q. Wang, T. Taniguchi, and G. H. Fredrickson, *J. Phys. Chem.* **108**, 6733 (2004).
- ²⁸Q. Wang, *Macromolecules* **38**, 8911 (2005).
- ²⁹P. Pincus, *Macromolecules* **24**, 2912 (1990).
- ³⁰S. J. Miklavic and S. Marčelja, *J. Phys. Chem.* **92**, 6718 (1988).
- ³¹S. Misra, S. Varanasi, and P. P. Varanasi, *Macromolecules* **22**, 4173 (1989).
- ³²F. von Goeler and M. Muthukumar, *Macromolecules* **28**, 6608 (1995).
- ³³H. Seki, Y. Y. Suzuki, and H. Orland, *J. Phys. Soc. Jap.* **76**, 104601 (2007).
- ³⁴K. N. Witte and Y.-Y. Won, *Macromolecules* **39**, 7757 (2006).
- ³⁵O. V. Borisov, F. A. M. Leermakers, G. J. Fleer, and E. Zhulina, *J. Chem. Phys.* **114**, 7700 (2001).
- ³⁶F. Zhou, P. M. Biesheuvel, E.-Y. Choi, W. Shu, R. Poetas, U. Steiner, and W. T. Huck, *Nanoletters* **8**, 725 (2008).
- ³⁷G. Parisi, *Statistical Field Theory* (Addison-Wesley, New York, 1988).
- ³⁸G. H. Fredrickson, *The Equilibrium Theory of Inhomogeneous Polymers* (Clarendon Press, Oxford, 2006).
- ³⁹M. Müller, *Phys. Rev. E* **65**, 030802 (2002).
- ⁴⁰J. U. Kim and M. W. Matsen, *Eur. Phys. J. E* **23**, 135 (2007).
- ⁴¹J. U. Kim and M. W. Matsen, *Macromolecules* **42**, 3430 (2009).
- ⁴²S. T. Milner, T. A. Witten, and M. E. Cates, *Macromolecules* **21**, 2610 (1988).
- ⁴³A. Johner and J.-F. Joanny, *J. Chem. Phys.* **98**, 1649 (1993).
- ⁴⁴E. B. Zhulina and O. V. Borisov, *J. Chem. Phys.* **107**, 5952 (1997).
- ⁴⁵F. Tricomi, *Pure and Applied Maths V: Integral Equations* (Interscience Publisher Inc. New York, 1957).
- ⁴⁶A. Semenov, *Sov. Phys. JETP* **61**, 733 (1985).
- ⁴⁷P. Henrici, *Discrete Variable Methods in Ordinary Differential Equations* (John Wiley, New York, 1962).
- ⁴⁸R. B. Thompson, K. Ø. Rasmussen, and T. Lookman, *J. Chem. Phys.* **120**, 31 (2004).

⁴⁹T. Taniguchi, Q. Wang, G. H. Fredrickson, M. Sugimoto, and K. Koyama, in *52nd Symp. Macromolecules* (Society of Polymer Science, Japan, ILL11, 2003).

⁵⁰A. Naji, R. R. Netz, and C. Seidel, *Eur. Phys. J. E* **12**, 223 (2002).

Appendix A: Partition function and Statistical field theory

In this appendix we review the basic formalism for a multicomponent polyelectrolyte system in solution. The saddle point equations (12) and (13) for a system of a single species of polyelectrolyte chains in the presence of counter-ions, discussed and studied in this paper are derived in detail in this Appendix and some simplifications, compared to a closely related derivation²⁵, are introduced. The average canonical partition function of an inhomogeneous multicomponent polyelectrolyte system is written^{25,38} as a functional integral over the cartesian position of the n_k small species, namely solvent molecules and counter-ions, over the conformation of charged polymer chains, belonging to n_p polymer distinct species, and finally over the charge distribution in the system, given the dimensionless polymer and small species concentrations in equations (1) and (2):

$$\langle \mathcal{Z} \rangle = \prod_p \left[\prod_{i=1}^{n_p} \sum_{\{z_p^i(s)\}} P(\{z_p^i(s)\}) \right] \mathcal{Z}(\{z_p^i(s)\}), \quad (\text{A1})$$

where

$$\begin{aligned} \mathcal{Z} &= \prod_j \left(\frac{\zeta_j^{n_j}}{n_j!} \right) \int \prod_p \left(\prod_i \mathcal{D}\mathbf{r}_p^i \right) \int \prod_k \left(\prod_i d\mathbf{r}_k^i \right) \\ &\times \exp \left(-\frac{\beta}{2} \rho_0^2 \sum_{jj'} \int d\mathbf{r} d\mathbf{r}' \hat{\phi}_j(\mathbf{r}) \mathcal{V}_{jj'}(\mathbf{r} - \mathbf{r}') \hat{\phi}_{j'}(\mathbf{r}') \right) \\ &\times \delta \left(\sum_j z_j N_j n_j \right) \prod_j \delta \left(\int d\mathbf{r} \hat{\phi}_j(\mathbf{r}) - n_j N_j \right) \\ &\times \prod_{\mathbf{r}} \delta \left(\sum_j \nu_j \hat{\phi}_j(\mathbf{r}) - 1 \right). \end{aligned} \quad (\text{A2})$$

In the expression above, the chain conformation path integral measure $\mathcal{D}\mathbf{r}^p = d\mathbf{r}^p P_{N_p}(\mathbf{r}^p)$,

$$P_{N_p}(\mathbf{r}_p^i) = \exp \left(-\frac{3}{2a^2} \int_0^{N_p} ds [\dot{\mathbf{r}}_p^i(s)]^2 \right), \quad (\text{A3})$$

is the Wiener measure, where N_p indicates the length of each polymer species, a is the Kuhn segment, $\zeta_j = \exp^{-\beta \rho_0^2 W_{jj}(0)} / \lambda_j^3$ is the reference chemical potential for species j , that includes the contact interaction energy and depends²⁵ on the thermal wave-length $\lambda_{T_j} = h / \sqrt{2\pi m_j k_B T}$. The canonical partition function has to be averaged over the charge distribution $P(\{z_p^i(s)\})$, characterizing each polyelectrolyte present in solution independently. The interaction energy term includes both short-ranged contact and long-ranged electrostatic interactions,

$$\begin{aligned} \mathcal{V}_{ij}(\mathbf{r} - \mathbf{r}') &= \mathcal{W}_{ij}(\mathbf{r} - \mathbf{r}') + \mathcal{E}_{ij}(\mathbf{r} - \mathbf{r}') \\ &= W_{ij} \delta(\mathbf{r} - \mathbf{r}') + \frac{e^2 z_i z_j}{\varepsilon(\mathbf{r}) |\mathbf{r} - \mathbf{r}'|}, \end{aligned} \quad (\text{A4})$$

where z_j is the valence of each species and should be considered as a function of s for any j that corresponds to a polymer species, where $\nu_j = \rho_o / \rho_j^o$ measures the different size of each molecule with respect to the reference density ρ_o , W_{ij} is the contact energy between species i and j , e is the elementary charge unit, $\varepsilon(\bar{r})$ the dielectric function and $\beta = 1/k_B T$ is the inverse temperature in Boltzmann units. The first two constraints in the above expression for the partition function relates to charge and particle conservation, while the last constraint refers to the incompressibility condition. We introduce the set of fields $\omega_j(\mathbf{r})$, $\phi_j(\mathbf{r})$ and express the canonical partition function in terms of a statistical field theory³⁷, using the particle-to-field transformation,

$$\begin{aligned} \langle \mathcal{Z} \rangle &= \int \prod_j [\mathcal{D}\omega_j \mathcal{D}\phi_j] \exp \left[-\beta \mathcal{H}(\{\omega_j\}, \{\phi_j\}) \right] \\ &\times \prod_{\mathbf{r}} \delta \left(\sum_j \nu_j \phi_j(\mathbf{r}) - 1 \right) \delta \left(\sum_j \bar{z}_j N_j n_j \right), \end{aligned} \quad (\text{A5})$$

where Stirling's formula has been used and where the canonical partition function is expressed in terms of the single species partition functions \mathcal{Q}_j , as an integral with respect to density and auxiliary fields of an effective Hamiltonian or 'action',

$$\begin{aligned} \beta \mathcal{H}(\{\omega_j\}, \{\phi_j\}) &= -i \rho_0 \sum_j \int d\mathbf{r} \omega_j(\mathbf{r}) \phi_j(\mathbf{r}) \\ &+ \frac{\beta \rho_0^2}{2} \sum_{jj'} \int d\mathbf{r} d\mathbf{r}' \phi_j(\mathbf{r}) \mathcal{V}_{jj'} \phi_{j'}(\mathbf{r}') \\ &- \rho_0 \sum_j \frac{\bar{\phi}_j V}{N_j} \ln \frac{\mathcal{Q}_j}{\bar{\phi}_j} + \rho_0 \sum_j \frac{\bar{\phi}_j V}{N_j} \ln \frac{\zeta_j N_j}{\rho_0} \end{aligned} \quad (\text{A6})$$

where $\bar{\phi}_j = N_j n_j / \rho_o V$ enforces the particle conservation constraint, where V is the volume, where the single species partition functions are:

$$\begin{aligned} \mathcal{Q}_k &= \frac{1}{V} \int d\mathbf{r} \exp \left\{ -i \int d\mathbf{r}^k \omega_k(\mathbf{r}) \right\} \\ \mathcal{Q}_p &= \frac{1}{V} \int \mathcal{D}\mathbf{r}^p(s) \sum_{\{z_p(s)\}} P(\{z_p(s)\}) \\ &\times \exp \left\{ -i \int_0^{N_p} ds [\omega_p(\mathbf{r}_p(s))] \right\}, \end{aligned} \quad (\text{A7})$$

and where finally we have considered the same charge distribution within each species being

$$\bar{z}_p = \int_0^1 ds z_p(s) P(z_p) = z_p f, \quad \bar{z}_k = z_k. \quad (\text{A8})$$

Both the smeared and the annealed charge distribution case are included in the present formulation, while the quenched distribution problem requires a different formulation. The saddle point equations corresponding to equation (A6), up to a redefinition of the fields ω_j are,

$$\begin{aligned} -i\omega_i - \frac{\beta\rho_o}{2} \sum_j \int d\mathbf{r}' \mathcal{V}_{ij}(\mathbf{r} - \mathbf{r}') \phi_i(\mathbf{r}') d\mathbf{r}' + \eta(\mathbf{r}) \nu_i &= 0 \\ -i\phi_i &= \frac{\bar{\phi}_i V}{N_j \mathcal{Q}_j} \frac{\delta \mathcal{Q}_j}{\delta \omega_j} \end{aligned} \quad (\text{A9})$$

where $\eta(\mathbf{r})$ is the Lagrange multiplier corresponding to the incompressibility constraint and where charge conservation applies: $\sum_j \bar{z}_j N_j n_j = 0$. The second set of saddle point equations, for the polymeric and small species, explicitly reads:

$$\begin{aligned} \phi_p &= \frac{\bar{\phi}_p}{\mathcal{Q}_p} \int_0^1 ds q_p(\mathbf{r}, s) q_p^\dagger(\mathbf{r}, s) \\ \phi_k &= \frac{\bar{\phi}_k}{\mathcal{Q}_k} \exp\{-i\omega_k(\mathbf{r})\} \end{aligned} \quad (\text{A10})$$

where the polymer propagator $q_p(\mathbf{r}, s)$ is the solution of the modified diffusion equation,

$$\begin{aligned} \frac{\partial}{\partial s} q_p(\mathbf{r}, \mathbf{r}_0, s) &= \frac{a^2 N_p}{6} \nabla^2 q_p(\mathbf{r}, \mathbf{r}_0, s) - i\omega_p(\mathbf{r}, s) q_p(\mathbf{r}, \mathbf{r}_0, s), \\ q_p(\mathbf{r}, \mathbf{r}_0, 1) &= (a^2 N)^{3/2} \delta(\mathbf{r} - \mathbf{r}_0). \end{aligned} \quad (\text{A11})$$

Integration of the Solvent Degrees of Freedom

It is useful to rewrite the effective hamiltonian in equation (A6) and the corresponding saddle point equations for the case where a single solvent species is present²⁵. One finds,

$$\begin{aligned} \beta\mathcal{H}(\{\omega_j\}, \{\phi_j\}) &= -i\rho_o \sum_j \int d\mathbf{r} \omega_j(\mathbf{r}) \phi_j(\mathbf{r}) \\ &+ \rho_o \sum_{jj'} \int d\mathbf{r} \chi_{jj'} \phi_j(\mathbf{r}) \phi_{j'}(\mathbf{r}) \\ &+ \frac{\beta\rho_o^2}{2} \sum_{jj'} \int d\mathbf{r} d\mathbf{r}' \phi_j(\mathbf{r}) \mathcal{E}_{jj'} \phi_{j'}(\mathbf{r}') \\ &- \rho_o \sum_j \frac{\bar{\phi}_j V}{N_j} \ln \frac{\mathcal{Q}_j}{\bar{\phi}_j} + \rho_o \sum_j \mu_{0j} \bar{\phi}_j, \end{aligned} \quad (\text{A12})$$

where,

$$\begin{aligned} \mu_{0j} &= \frac{\beta\rho_o}{2} \left[W_{jj} - \frac{1}{N_j} \ln \left(\frac{\zeta_j Z_j}{\rho_o} \right) \right] \\ \chi_{ij} &= \frac{\beta\rho_o}{2} \left[2W_{ij} - \left(\frac{\nu_j}{\nu_i} W_{ii} + \frac{\nu_i}{\nu_j} W_{jj} \right) \right]. \end{aligned} \quad (\text{A13})$$

The saddle point equations for the solvent degrees of freedom can be integrated out. In the semi-dilute regime²⁵, the saddle point equation for the partition function \mathcal{Q}_s defined in equation (A10) can be expanded to obtain,

$$i\omega_s \simeq \sum_{j \neq s} \nu_j \phi_j, \quad (\text{A14})$$

where the primed sum is over all species but the solvent species. The Lagrange multiplier $\eta(\mathbf{r})$ can be written as

$$\eta(\mathbf{r}) \nu_s = \sum_{j \neq s} (\nu_j - \chi_{js}) \phi_j(\mathbf{r}) \quad (\text{A15})$$

so that a new set of reduced saddle point equations, with $i \neq s$, holds

$$\begin{aligned} -i\omega_i + \sum_{j \neq s} v_{ij} \phi_j(\mathbf{r}) + \frac{\beta\rho_o}{2} \sum_j \int d\mathbf{r}' \mathcal{E}_{ij}(\mathbf{r}' - \mathbf{r}) \phi_j(\mathbf{r}) \\ -i\phi_i &= \frac{\bar{\phi}_i V}{N_j \mathcal{Q}_j} \frac{\delta \mathcal{Q}_j}{\delta \omega_j}, \end{aligned} \quad (\text{A16})$$

where $v_{ij} = \left(\frac{\nu_i \nu_j}{\nu_s} - \chi_{ij} \right)$, where the index j is intended to run over all species excluding the solvent and where finally the Flory parameter between species i and j is defined in equation (A13).

Appendix B: Derivation of Model Details

We consider explicitly the case where we can neglect the excluded-volume interactions of the small species. For two distinct indices for the polymeric and small species, considering the dielectric constant to be uniform across the system and considering the case of a smeared polyelectrolyte charged distribution, with charged ion fraction parameter f , we find:

$$\begin{aligned} i\omega_k(\mathbf{r}) &= \rho_o \frac{\beta e^2}{2} z_c \int d\mathbf{r}' \frac{\sum_j z_j \phi_j(\mathbf{r}')}{\epsilon |\mathbf{r} - \mathbf{r}'|}, \\ i\omega_p(\mathbf{r}) &= \sum_{p'} v_{pp'} \phi_{p'}(\mathbf{r}) + i \frac{z_p}{z_k} f \omega_k \end{aligned} \quad (\text{B1})$$

where $i\omega_c$ is related to the dimensionless electrostatic potential $\psi(\mathbf{r})$ according to $\psi(\mathbf{r}) = i\omega_k(\mathbf{r}) z_k$. Let us consider the case of a single polymer species, and let us consider a single species of point particles: in this case the

above saddle point equations reduce to

$$\begin{aligned} i\nabla^2\omega_c(\mathbf{r}) &= -4\pi l_B\rho_0z_c\sum_j z_j\phi_j(\mathbf{r}) \\ i\omega_p(\mathbf{r}) &= v\phi_p(\mathbf{r}) + i\frac{z_p}{z_c}f\omega_c(\mathbf{r}). \end{aligned} \quad (\text{B2})$$

The corresponding mean-field free-energy can be computed according to equation (A6). The canonical Model F field theory partition function³⁸ reads:

$$\langle \mathcal{Z} \rangle = \mathcal{Z}_0 \int D\omega_p D\omega_c \exp \left\{ -\beta\mathcal{H}[\omega_p, \omega_c] \right\} \quad (\text{B3})$$

where

$$\begin{aligned} \beta\mathcal{H}[\omega_p, \omega_c]/\rho_0 &= \frac{1}{2v} \int d\mathbf{r} (\omega_p - \frac{z_p}{z_c}f\omega_c)^2 \\ &+ \frac{1}{8\pi l_B z_c^2} |\nabla\omega_c|^2 - \frac{n_p}{V} \ln \mathcal{Q}_p[i\omega_p] - \frac{n_c}{V} \ln \mathcal{Q}_c[i\omega_c] \end{aligned} \quad (\text{B4})$$

and where the partition function,

$$\mathcal{Z}_0 = \exp\{\bar{\phi}_p \ln \bar{\phi}_p + \bar{\phi}_c \ln \bar{\phi}_c + \mu_{0p} V \bar{\phi}_p + \mu_{0c} V \bar{\phi}_c\}, \quad (\text{B5})$$

also written as

$$\mathcal{Z}_0 = \frac{\zeta_p^{n_p} \zeta_c^{n_c}}{n_p! n_c!} e^{\beta/2W_{pp}}, \quad (\text{B6})$$

is the ideal non-interacting partition function of a mixture of n_p charged polymers and n_c counter-ions in solution. Changing variables we write,

$$\begin{aligned} \beta\mathcal{H}[\omega, \omega_c] &= \int d\mathbf{r} \frac{1}{2v} \omega^2 + \frac{1}{8\pi l_B z_c^2} |\nabla\omega_c|^2 \\ &- n_p \ln \mathcal{Q}_p[i\omega + i\frac{z_p}{z_c}f\omega_c] - n_c \ln \mathcal{Q}_c[i\omega_c]. \end{aligned} \quad (\text{B7})$$

The saddle point free-energy is

$$\begin{aligned} \frac{F}{k_B T} &= \beta\mathcal{H}[-i\omega, -i\psi]/\rho_0 = \frac{1}{8\pi l_B} \int d\mathbf{r} |\nabla\psi(\mathbf{r})|^2 \\ &- \frac{1}{2v} \int d\mathbf{r} \omega^2(\mathbf{r}) - n_p \ln \mathcal{Q}_p[w_p + \bar{z}_p\psi] - n_c \ln \mathcal{Q}_c, \end{aligned} \quad (\text{B8})$$

where v is the excluded-volume parameter and where $l_B = e^2/k_B T \epsilon$ is the Bjerrum length. Note that the electrostatic interaction energy term can be rewritten, using equation (B2),

$$\begin{aligned} \frac{F}{k_B T} &= -\frac{1}{2v} \int d\mathbf{r} \omega^2(\mathbf{r}) - \frac{1}{2} \int d\mathbf{r} \psi(\mathbf{r}) (\phi_p(\mathbf{r}) - \phi_c(\mathbf{r})) \\ &- n_p \ln \mathcal{Q}_p[w_p + z_p f \psi] - n_c \ln \mathcal{Q}_c[\psi]. \end{aligned} \quad (\text{B9})$$

Equation (B9), after a few steps can be shown to reduce to the free-energy expression discussed in equation (25).

Appendix C: On Abel-Volterra equations of the second kind

In this section we give a detailed derivation of the integral Abel-Volterra equations of the first and second kind discussed in section VI. Consider the integral equation

$$\int_U^{U_0} dt f(t) (t-U)^{-1/2} = g(U). \quad (\text{C1})$$

We write¹³,

$$\begin{aligned} &\int_\eta^U dU_0 g(U_0) (U_0 - \eta)^{-1/2} = \\ &\int_\eta^U dU_0 (U_0 - \eta)^{-1/2} \int_U^{U_0} dt f(t) (t-U)^{-1/2}. \end{aligned} \quad (\text{C2})$$

Using Fubini's theorem we find,

$$\begin{aligned} &\int_\eta^{U_0} dU g(U) (U - \eta)^{-1/2} = \\ &\int_\eta^{U_0} dt f(t) \int_\eta^t dU (U - \eta)^{-1/2} (t - U)^{-1/2}. \end{aligned} \quad (\text{C3})$$

According to the assumption of strong-stretching theory, one neglects the chain end tension $V_0 \approx 0$; the parabolic form in equation (33) follows considering the constraint in equation (30), corresponding to $g(U) = 1$ in equation (C1). This yields

$$f(\eta) = \frac{1}{\pi} (U_0 - \eta)^{-1/2}, \quad (\text{C4})$$

that can be integrated to obtain the parabolic form in equation (34). Similarly, an expression for the end-monomer distribution can be obtained considering

$$\int_Z^H dZ_0 g(Z_0) (Z_0^2 - Z^2)^{-1/2} = \frac{\pi}{2} \phi_p(Z) \quad (\text{C5})$$

and inverting this expression^{13,44} by fractional differentiation,

$$f(U) = -\frac{1}{\pi} \frac{d}{dU} \int_U^{U_0} dt g(t) (t-U)^{-1/2}, \quad (\text{C6})$$

one finds equation (42). As discussed in section VI, let us consider now the case of a uniform tension at the chain ends. The integral form in equation (C3) can be written as

$$\begin{aligned} &\int_\eta^{U_0} dU (U - \eta)^{-1/2} = \\ &\int_\eta^{U_0} dt f(t) \left\{ \frac{\pi}{2} + \arcsin \left(\frac{(t-\eta) - V_0^2}{(t-\eta) + V_0^2} \right) \right\}. \end{aligned} \quad (\text{C7})$$

Expanding to leading order yields an Abel Integral equation of the second kind,

$$\int_{\eta}^{U_0} dU (U - \eta)^{-1/2} = \int_{\eta}^{U_0} dt f(t) \left\{ \pi - \alpha (t - \eta)^{-1/2} \right\}, \quad (\text{C8})$$

where $\alpha = \sqrt{6}|V_0|$ measures the uniform end-monomer tension induced by the electric field, as discussed in section VI. We find:

$$\begin{aligned} f(\eta) + \frac{\alpha}{\pi} \frac{d}{d\eta} \int_{\eta}^{U_0} dt f(t) (t - \eta)^{-1/2} \\ = -\frac{1}{\pi} \frac{d}{d\eta} \int_{\eta}^{U_0} dt (t - \eta)^{-1/2}. \end{aligned} \quad (\text{C9})$$

This can be written as

$$f(\eta) = -\frac{1}{\pi} \frac{d}{d\eta} \int_{\eta}^{U_0} (1 + \alpha f(t)) (t - \eta)^{-1/2} dt, \quad (\text{C10})$$

and

$$\int_{\eta}^{U_0} f(t) (t - \eta)^{-1/2} dt = \alpha f(\eta) - 1. \quad (\text{C11})$$

The presence of the external field converts the Abel-Volterra integral equation of the first kind (C1), as usually discussed within strong-stretching theory, to an integral equation of the second kind (C9). The integral equation (C9) can be solved and a new form of the potential follows, as we will show in the rest of this Appendix. To leading order in the Taylor expansion, we find

$$\begin{aligned} \frac{df(\eta)}{d\eta} - \frac{\pi}{\alpha^2} f(\eta) &= \frac{d}{d\eta} F(\eta) \\ F(\eta) &= g(\eta) - \frac{1}{\alpha} \int_{\eta}^{U_0} dt g(\eta) (t - \eta)^{-1/2}. \end{aligned} \quad (\text{C12})$$

The isochronicity constraint in equation (31) requires the function $g(\eta)$ to be constant, namely $g(\eta) = -1/\alpha$, so that

$$F(\eta) = -\frac{1}{\alpha} + \frac{2}{\alpha^2} (U_0 - \eta)^{1/2}, \quad (\text{C13})$$

and the solution to the Abel-Volterra integral equation of the second kind (C9) has the form

$$f(\eta) = F(\eta) + \frac{\pi}{\alpha^2} \int_{\eta}^{U_0} dt e^{\frac{\pi}{\alpha^2}(U_0-t)} F(t) \quad (\text{C14})$$

and after a few steps we find

$$f(\eta) = \frac{1}{\alpha} e^{\frac{\pi}{\alpha^2}(U_0-\eta)} \frac{1}{\sqrt{\pi}} \Gamma\left(\frac{1}{2}, \frac{\pi}{\alpha^2}(U_0 - \eta)\right), \quad (\text{C15})$$

where $\Gamma(\alpha, x)$ is the incomplete gamma function of order 1/2 and where the potential form can be obtained integrating equation (C15). We note that the function $f(U) = \sqrt{\frac{3}{2}} dZ/dU$ can be written as

$$f(\eta) = \frac{1}{\alpha \sqrt{\pi}} \mathcal{U}\left(\frac{1}{2}, \frac{1}{2}, \frac{\pi}{\alpha^2}(U_0 - \eta)\right), \quad (\text{C16})$$

where $\mathcal{U}\left(\frac{1}{2}, \frac{1}{2}, \frac{\pi}{\alpha^2}(U_0 - \eta)\right)$ is the confluent hypergeometric Tricomi function and where one recovers the standard strong-stretching theory prediction to first order expansion. It is easily checked that the first order in the above mentioned expansion corresponds to the strong-stretching theory result:

$$f(\eta) = \frac{1}{\pi} (U_0 - \eta)^{-1/2}, \quad (\text{C17})$$

that corresponds to the parabolic form (34). Equation (C15) can be integrated, and one finds

$$\sqrt{\frac{3}{2}} \pi Z = \frac{\alpha}{\sqrt{\pi}} \int_0^{\frac{\pi}{\alpha^2}(U_0-U)} \Gamma\left(\frac{1}{2}, t\right) e^t dt, \quad (\text{C18})$$

and finally

$$\begin{aligned} \sqrt{\frac{3}{2}} \pi Z &= 2(U_0 - U)^{1/2} + \alpha - \frac{\alpha}{\sqrt{\pi}} e^{\frac{\pi}{\alpha^2}(U_0-U)} \\ &\times \Gamma\left(\frac{1}{2}, \frac{\pi}{\alpha^2}(U_0 - U)\right). \end{aligned} \quad (\text{C19})$$

The above expression has been used to obtain the potential, for both negative and positive values of the chain-end force, shown in Fig. 11 and discussed in section VI. For the chain end distribution we find

$$\begin{aligned} \frac{ds(\eta)}{d\eta} - \frac{\pi}{\alpha^2} s(\eta) &= \frac{d}{d\eta} G(\eta) \\ G(\eta) &= -\frac{1}{\alpha} \eta + \frac{4}{3\alpha^2} \eta^{3/2}, \end{aligned} \quad (\text{C20})$$

where $s(\eta) = g(\eta) \frac{dZ}{d\eta}$. The expression for the chain-end distribution in equation (47) can be obtained solving the above second kind Abel-Volterra integral equation as well as using the result of equation (C15) above.